Developing a deep learning-based imaging diagnostic framework, PVDNet, for differentiating pulmonary artery sarcoma and pulmonary thromboembolism: a multi-center observational study

Linfeng Xi,[a,b,z] Anqi Liu,[c,d,z] Han Kang,[e,z] Yifei Ni,[c,d] Jianping Wang,[a,c] Hongyi Wang,[b,d] Xiaoyan Li,[f] Xiaojuan Guo,[g] Minjie Lu,[h] Hui Liu,[i] Yinzhu Chen,[j,i] Heng Ma,[k] Yinsu Zhu,[l] Yu Deng,[m] Liqing Peng,[n] Fajiu Li,[o] Ziyang Zhu,[o] Lihua Wang,[p] Xin Chen,[q] Hong Yu,[r] Hongjie Hu,[s] Cong Shen,[t] Xiaoyan Lei,[u] Zixian Chen,[v] Xincao Tao,[w] Qiang Huang,[b] Xiaopeng Liu,[x] Yanan Zhen,[x] Rongguo Zhang,[y] Wanmu Xie,[b] Zhenguo Zhai,[b,**] and Min Liu,[c,*] on behalf of the CHinese PE multimOdality Imaging artifiCial intElligence (CHOICE) Investigators

[a]China-Japan Friendship Hospital, Capital Medical University, Beijing, 100069, China
[b]National Center for Respiratory Medicine, State Key Laboratory of Respiratory Health and Multimorbidity, National Clinical Research Center for Respiratory Diseases, Institute of Respiratory Medicine, Chinese Academy of Medical Sciences, Department of Pulmonary and Critical Care Medicine, Center of Respiratory Medicine, China-Japan Friendship Hospital, Beijing, 100029, China
[c]Department of Radiology, China-Japan Friendship Hospital, Beijing, 100029, China
[d]Chinese Academy of Medical Sciences and Peking Union Medical College, Beijing, 100730, China
[e]Institute of Advanced Research, Infervision Medical Technology Co., Ltd., Beijing, 100025, China
[f]Department of Radiology and Interventional Radiology, The Red Cross Hospital in Qinghai, Xining, 810000, China
[g]Department of Radiology, Beijing Chao-Yang Hospital, Capital Medical University, Beijing, 100020, China
[h]Department of Magnetic Resonance Imaging, Fuwai Hospital and National Center for Cardiovascular Diseases, Chinese Academy of Medical Sciences and Peking Union Medical College, Beijing, 100037, China
[i]Department of Radiology, Guangdong Provincial People's Hospital, Southern Medical University, Guangzhou, 510080, China
[j]School of Medicine, South China University of Technology, Guangzhou, 510006, China
[k]Department of Radiology, Yantai Yuhuangding Hospital, Qingdao University, Yantai, Shandong, 264009, China
[l]Department of Radiology, Affiliated Cancer Hospital of Nanjing Medical University, Jiangsu Cancer Hospital, Jiangsu Institute of Cancer Research, Nanjing, 210009, China
[m]Department of Radiology, The First Affiliated Hospital of Guangzhou Medical University, Guangzhou, 510120, China
[n]Department of Radiology, West China Hospital, Sichuan University, Chengdu, 610041, China
[o]Department of Respiratory Medicine, Wuhan No. 6 Hospital, Affiliated Hospital to Jianghan University, Wuhan, 430072, China
[p]Department of Radiology, The Second Affiliated Hospital, Zhejiang University School of Medicine, Hangzhou, 310009, China
[q]Department of Radiology, The Second Affiliated Hospital of Xi'an Jiaotong University, Xi'an, 710004, China
[r]Department of Radiology, Shanghai Chest Hospital, Shanghai Jiao-Tong University, Shanghai, 200030, China
[s]Department of Radiology, Sir Run Run Shaw Hospital, School of Medicine, Zhejiang University, Hangzhou, 310018, China
[t]Department of PET/CT, The First Affiliated Hospital of Xi'an Jiaotong University, Xi'an, 710061, China
[u]Department of MRI, Shaanxi Provincial People's Hospital, Xi'an, 710068, China
[v]Department of Radiology, The First Hospital of Lanzhou University, Lanzhou, 730000, China
[w]Chinese Academy of Medical Sciences Fuwai Hospital Center for Respiratory and Pulmonary Vascular Diseases, Beijing, 100037, China
[x]Department of Cardiovascular Surgery, China-Japan Friendship Hospital, Beijing, 100029, China
[y]Academy for Multidisciplinary Studies, Capital Normal University, Beijing, 100080, China

Summary

Background **Differentiating pulmonary artery sarcoma (PAS) from pulmonary thromboembolism (PTE) based on CT pulmonary angiography (CTPA) is a big challenge, necessitating the incorporation of other methods, such as deep learning (DL). This study aimed to develop and validate a DL-based model, PVDNet, for differentiating PAS and PTE on CTPA.**

The Lancet Regional Health - Western Pacific 2025;60: 101625

Published Online 10 July 2025
https://doi.org/10.1016/j.lanwpc.2025.101625

*Corresponding author. Department of Radiology, China-Japan Friendship Hospital, No 2 East Yinghua Road, Hepingli, Chaoyang District, Beijing, 100029, China.
**Corresponding author. Department of Pulmonary and Critical Care Medicine, China-Japan Friendship Hospital, National Center for Respiratory Medicine, Institute of Respiratory Medicine, Chinese Academy of Medical Sciences, National Clinical Research Center for Respiratory Diseases, No 2 East Yinghua Road, Hepingli, Chaoyang District, Beijing, 100029, China.
E-mail addresses: mikie0763@126.com (M. Liu), zhaizhenguo2011@126.com (Z. Zhai).
[z]Linfeng Xi, Anqi Lu, and Han Kang ciontributed equally and shared the first authorship.

Methods This study retrospectively analyzed CTPA image datasets from the prospective CHinese pulmOnary embolism multimodality Imaging artifiCial intelligencE (CHOICE) study to develop and validate a DL model for differentiating PAS from PTE. CTPA image datasets of 952 patients (470 acute PTE [APE], 363 chronic PTE [CPE], and 119 PAS) from 15 hospitals were included. The training set comprised CTPA images from 590 patients, and the internal test set comprised those from 186 patients, all obtained from the same three centers. CTPA images of 176 patients from 12 centers were used for external validation. A DL framework, PVDNet, was employed to perform fine-grained classification. Meanwhile, CTPA images in the external validation set were independently assessed by four radiologists with different levels of expertise. The main outcome measures were area under the curve (AUC) and the consistency test.

Findings In the internal test set, PVDNet achieved an AUC of 0.972, 0.902, and 0.900 for PAS (95% CI: [0.945, 0.994]), APE (95% CI: [0.855, 0.944]), and CPE (95% CI: [0.852, 0.946]), respectively. Furthermore, PVDNet model demonstrated effective differentiation between PAS and PTE, showing comparable AUC values to a senior radiologist specialized in pulmonary vascular diseases (SRPV) in the external validation set (0.973 vs. 0.943, $p = 0.308$). The model achieved moderate agreement with SRPV (kappa = 0.651, $p < 0.001$), which was the highest among four readers.

Interpretation PVDNet model could differentiate PAS from PTE, with performance approaching the proficiency level of a senior radiologist specializing in pulmonary vascular diseases. PVDNet's performance in distinguishing APE from CPE requires further optimization.

Funding National Natural Science Foundation of China (No. 82272081), Medical and Health Science and Technology Innovation Project of Chinese Academy of Medical Science (No. 2021-I2M-1-049), and the National Key Research and Development Program of China (No. 2023YFC2507200).

Keywords: Pulmonary thromboembolism; Pulmonary artery sarcoma; Computed tomography pulmonary angiography; Deep learning

Research in context

Evidence before this study

We searched PubMed and Google Scholar database up to November 30, 2024, for papers published in English, using the terms "pulmonary embolism", "pulmonary artery sarcoma", "computed tomography pulmonary angiography", "deep learning". Our search showed that previous studies mainly focused on the clinical and imaging characteristics, and outcomes of pulmonary artery sarcoma (PAS) and pulmonary thromboembolism (PTE), indicating that PAS can mimic PTE. These studies are primarily case reports, observational studies, or systematic reviews. However, a deep learning-based model for differential diagnosis of PAS from PTE is still lacking.

Added value of this study

To our knowledge, this is the first imaging model to differentiate PAS from PTE based on deep learning. Our PVDNet model provides an option to improve the efficiency and accuracy of radiologists' work, and may lead to early referral to pulmonary vascular disease centers for advanced PAS evaluation and intervention.

Implications of all the available evidence

The PVDNet model based on CTPA improved the efficiency and accuracy of differentiating PAS from PTE, which had the potential to reduce diagnosis delay and improve the prognosis of PAS patients. Additionally, the model could assist less experienced radiologists in making more precise diagnoses of PAS.

Introduction

Pulmonary thromboembolism (PTE) is the third leading cause of cardiovascular disease-related deaths after myocardial infarction and stroke.[1] However, the mortality rate of acute PTE (APE) has declined due to advancements in techniques for timely diagnosis and development of effective therapies.[2,3] Chronic PTE (CPE) is a long-term complication of venous thromboembolism, which can potentially progress to chronic thromboembolic pulmonary hypertension. The treatment for CPE differs from that of APE.[4–7] Computed tomography pulmonary angiography (CTPA) has been widely used for PTE diagnosis because it can effectively reveal the filling defects in pulmonary arteries.

However, filling defects in the pulmonary arteries may not always indicate the presence of PTE. Pulmonary artery sarcoma (PAS) is rare and originates from the pulmonary artery with poor prognosis.[8–10] Early PAS diagnosis prevents inappropriate anticoagulation duration and allows for timely surgical intervention, potentially improving outcomes. However, since PAS also manifests as filling defects in the pulmonary arteries on CTPA, it frequently causes to misdiagnosis during patients' first consultations and inappropriate anticoagulation. Previous studies have attempted to distinguish PAS from PTE using imaging findings, but the number of patients included in such studies was too small and the imaging findings were nonspecific.[10–16] Although 18F-FDG PET/CT and MRI can effectively differentiate PAS from PTE, their use as initial imaging examinations remains challenging for most patients with suspected pulmonary vascular diseases.[12,13,16,17]

With the advance of artificial intelligence (AI) in medical imaging, its introduction to clinical workflow has been proposed to facilitate the diseases diagnosis and treatment. Deep learning (DL) model has been used to evaluate APE,[18,19] differentiate constrictive pericarditis from restrictive cardiomyopathy, hypertrophic cardiomyopathy and hypertensive heart disease,[20–22] and to segment and predict percutaneous recanalization in chronic total occlusion on coronary CT angiography.[23,24] However, a DL-based model for differential diagnosis of PAS from PTE is still lacking. We aimed to develop and validate a DL model which could accurately differentiate PAS from PTE based on CTPA.

Methods

Study design and cohort

The CHinese pulmOnary embolism multimodality Imaging artifiCial intelligencE Study (CHOICE) is a prospective, observational, and multicenter study registered at ClinicalTrials.gov (NCT06526468). This study developed a DL model through retrospective analysis of CTPA imaging datasets. To ensure clinical relevance and mitigate data leakage, we adopted a non-random, center- and time-based splitting strategy for dataset partitioning. The training set comprised CTPA images from three centers collected between January 2015 and December 2019, while the internal test set included studies from the same centers but restricted to January 2020–December 2023. This temporal separation simulates real-world model deployment, where future data distributions may differ from historical training data. The external validation set was sourced from the other 12 independent centers from January 2021 to December 2023, further testing generalizability across diverse clinical settings and scanner types. The study adhered to the guidelines outlined in the TRIPOD-AI checklist[25] (*TRIPOD-AI checklist*), ensuring transparency and reproducibility of predictive models in AI research.

The inclusion criteria were: I. Patients with central-type filling defects on CTPA (filling defects located in the lobe or larger pulmonary artery), including APE, CPE, and PAS:

Ia. APE diagnosis required: (1) Baseline CTPA-confirmed intraluminal filling defects; (2) Corroborative clinical/laboratory evidence; (3) Symptomatic and laboratory improvement after ≥3-month anticoagulation, or follow-up CTPA suggesting a significant reduction in intraluminal filling defects, or follow-up ventilation-perfusion (V/Q) scintigraphy suggesting a significant reduction in perfusion defects.

Ib. CPE was defined by: (1) Persistent exertional symptoms despite ≥3 months of effective anticoagulation; (2) V/Q scintigraphy showing ≥2 mismatched segmental/lobar perfusion defects; (3) CTPA/pulmonary angiography confirming chronic thromboembolic signs; (4) Patients who underwent BPA treatment (n = 169) or PEA (n = 145) were included.

Ic. PAS patients confirmed via endovascular biopsy or surgical pathology. All ambiguous cases underwent adjudication by a multidisciplinary panel.

Exclusion criteria included: I. CTPA with poor image quality or severe artifacts. II. CTPA without Digital Imaging and Communications in Medicine Format (DICOM). III. Patients who were lost to follow-up or diagnosed with other types of pulmonary embolism, including fibrinous mediastinitis, Takayasu arteritis, Bechet's disease, hydatid pulmonary embolism, and pulmonary artery lipoma.

Initially, 1587 consecutive CTPA studies were collected from 15 participating centers. According to exclusion criteria, 635 cases were excluded (detailed in Fig. 1). The remaining 952 eligible CTPA studies were ultimately included for model development and validation. CTPA image dataset from 952 patients (male 542, Mean age = 61.1 ± 15.4 years) diagnosed with APE, CPE, and PAS from 15 imaging centers were included in this study. 590 CTPA studies from 590 patients (January 2015–December 2019; 390,816 slices) and 186 studies from 186 patients (January 2020–December 2023; 65,198 slices) across three centers served as training and internal test sets, respectively. An external validation set comprised 176 patients (a total of 60,720 slices) from 12 additional centers between January 2021 and December 2023.

CTPA scan protocol

Various multidetector CT scanners (Siemens: SOMATOM Sensation 64, SOMATOM Definition AS, SOMATOM Definition Edge, SOMATOM Definition Flash, SOMATOM Force; GE Healthcare: GE LightSpeed VCT, GE Optima CT660, Discovery CT750 HD, Revolution CT; Philips: Brilliance 64, Brilliance ICT, Ingenuity CT 64, Ingenuity Core128; The Canon

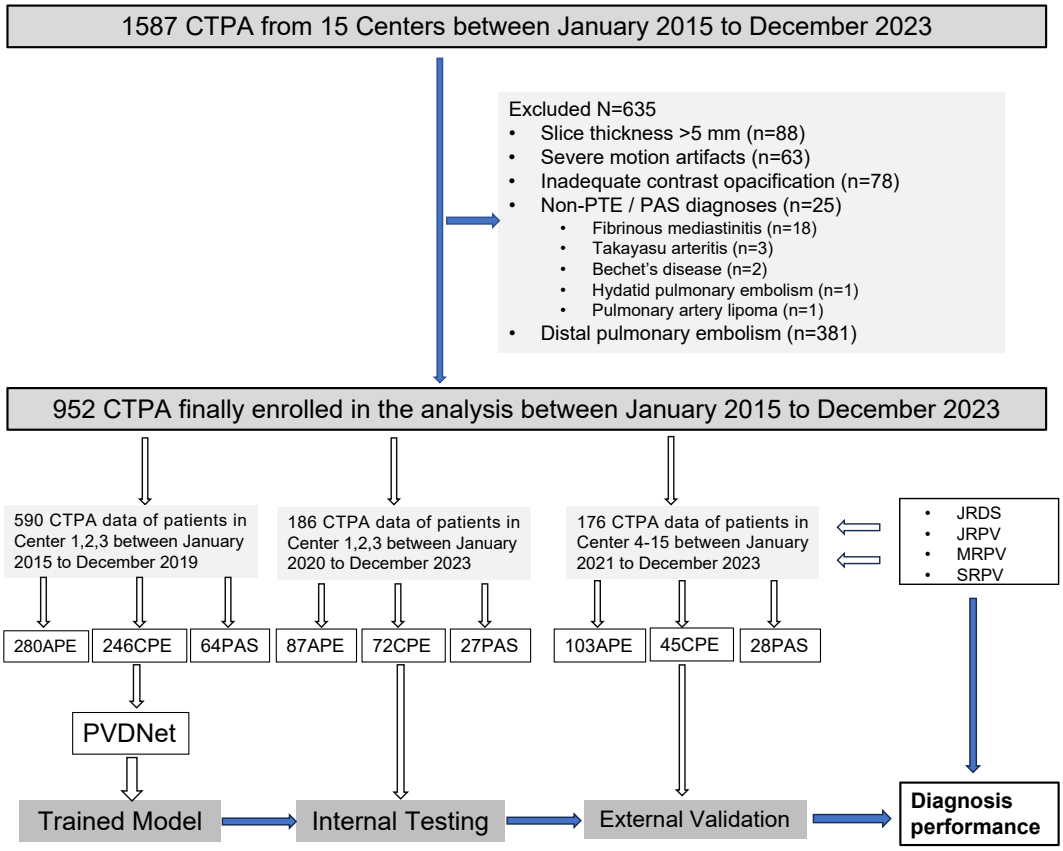

Fig. 1: Flowchart of the multicenter study. A total of 1587 CTPA datasets were collected from 15 medical centers between January 2015 and December 2023. After applying exclusion criteria, 88 cases were excluded due to slice thickness >5 mm, 63 due to severe motion artifacts, 78 due to inadequate contrast opacification, 25 cases with final diagnoses unrelated to PTE or PAS, and 381 due to peripheral pulmonary embolism. Thus, CTPA image dataset of 952 patients was included. The dataset was split into training set and internal testing set at the patient level. A total of 590 and 186 CTPA images were included for model development and internal testing. A supervised deep learning framework (PVDNet) was constructed to classify PAS, APE, and CPE. The performance of the model was evaluated using an independent external validation set (n = 176) and compared with four radiologists. CTPA = computed tomography pulmonary angiography; PAS = pulmonary artery sarcoma; PTE = pulmonary thromboembolism; APE = acute pulmonary thromboembolism; CPE = chronic pulmonary thromboembolism; JRDS = a junior resident with 3 years of experience; JRPV = a junior radiologist with 6 years of experience in pulmonary vascular diseases; MRPV = a mid-career radiologist with 13 years of experience in pulmonary vascular diseases; SRPV = a senior radiologist with 20 years of experience in pulmonary vascular diseases.

Aquilion CXL; United Imaging Healthcare: uCT 780) were used for CTPA scanning (detailed in Appendix Table S1).

The entire chest was scanned from lung apex to the diaphragm during a single breath-hold. Scan parameters included: tube current 300–550 mA, tube voltage 100–120 kV, detector collimation 0.625–1 mm, and reconstruction increment 1 mm. A high-pressure injector was used for intravenous bolus injection of the iopromide at 4.0–4.5 ml/s. The automatic bolus-tracking technique was implemented during the injection, with a region of interest defined within the main pulmonary artery using a pre-determined threshold of 80–100 Hounsfield Units (HU). To avoid biases caused by multicenter studies and different scanners, we performed data standardization (see Appendix Material 1 for details).

Image preprocessing

Before training model, all CTPA image datasets in DICOM format were preprocessed through several steps (Fig. 2A). First, all images were processed with unified window width and level parameters (window center: 100 HU, window width: 700 HU), ensuring that images obtained from different centers and scanners had similar contrast characteristics. Second, the lung mask was automatically extracted by a DL-based segmentation method provided by a medical imaging solution software (InferRead™ CT Lung, version R3.12.3; Infervision Medical Technology Co., Ltd., Beijing,

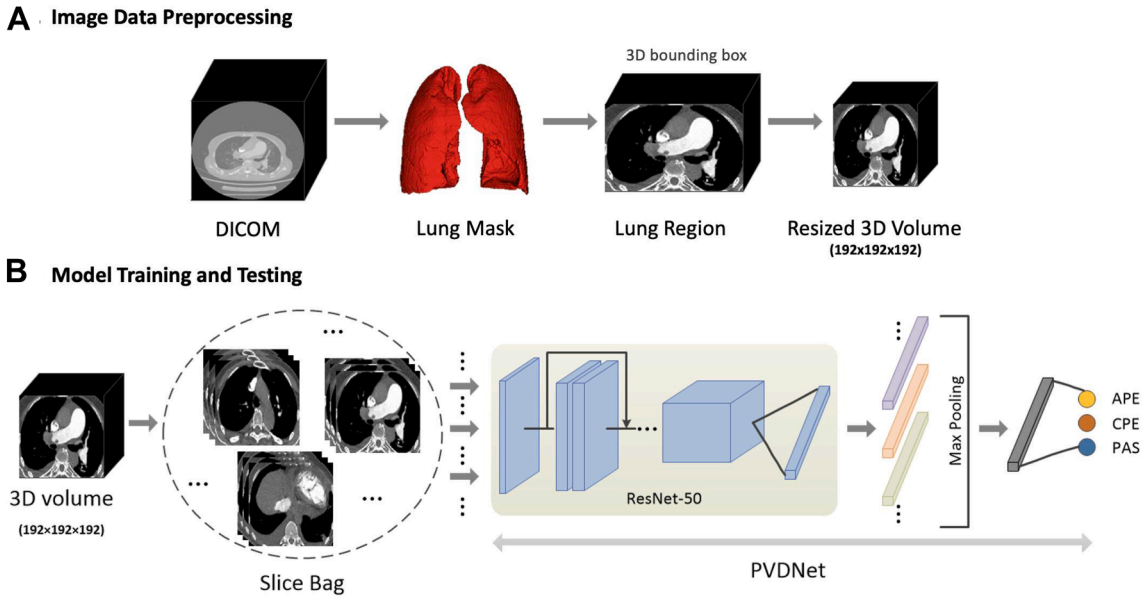

Fig. 2: The workflow of the PVDNet model. (A) First, CTPA scan was preprocessed to extract the lung mask and lung region (192 × 192 × 192 3D) via resizing operation. (B) The 3D volume was split, and a 2D slice bag was formed using 192 three-channel images. The PVDNet was used for class prediction. In this network, the ResNet-50 was employed to extract instance features from each three-channel image. The obtained features were simultaneously passed into a max pooling layer for feature aggregation, and the features were fed into a fully connected layer using the softmax function to get a probability score for each class. DICOM = digital imaging and communications in medicine format; APE = acute pulmonary thromboembolism; CPE = chronic pulmonary thromboembolism; PAS = pulmonary artery sarcoma.

China),[26] as described in Appendix Material 1. Third, the lung region was extracted from each CT scan via a 3D bounding box derived from the corresponding segmentation mask, preserving the pulmonary arteries and heart. Fourth, to meet the training requirements of ResNet-50, each lung region was resized to 192 × 192 × 192. The resized lung regions were subjected to min–max normalization, further reducing the gray–level differences that might be caused by different scanning parameters.

Deep learning model

Based on the COVNet model,[27] a supervised convolutional neural network framework was employed to perform fine-grained classification. The proposed framework (Fig. 2B) utilizes the pre-trained ResNet-50,[28] a 50-layer residual DL model with 3.8 billion trainable parameters, to extract instance features. The weights of the ResNet-50 in the COVNet was pretrained by ImageNet,[29] and the classification layer (the fully connection layer) was initialized by the Kaiming method. The whole network was trained on 50 epochs using Adam optimizer with the initial learning rate of $1e^{-5}$ and the mini-batch size of 1. The stochastic gradient descent optimizer with a momentum of 0.9 was utilized to accelerate convergence while overcoming local minima. Considering the small sample size of PAS in the training set, we used class-balanced sampling to mitigate the effect of class imbalance and selected the class-balanced loss[30] as the loss function to address the issue of data imbalance (Appendix Material 2). During training, we adopted ReduceLROnPlateau method based on the loss of the tuning set to adjust learning rate. Data augmentation was performed by the toolkit named batchgenerators.[31] A max-pooling operation is employed for feature aggregation, followed by a fully connected layer. The shallow layers of ResNet-50 (Conv1 to Conv2_x) were frozen to retain the general feature extraction learned during pre-training, while deeper layers (Conv3_x and beyond) were fine-tuned on CTPA image data to optimize performance for pulmonary vascular diseases. A softmax activation function is applied to generate probability scores for each class (APE, CPE, and PAS). Specifically, the CTPA dataset for each patient was first preprocessed, followed by splitting of the preprocessed image along the z-axis. Each image slice was copied into a three-channel image, considered as a 2D instance. All instances were formed as a slice bag. Each three-channel image in the bag was passed to the model for the classification diagnosis. Since this ResNet-50-based model will be used for the classification diagnosis of pulmonary vascular diseases, we named it PVDNet. In the training phase, the model performance on the tuning set was assessed by macro F1 score. In our study, the mean F1 score of five selected models on the tuning set was 0.838 ± 0.051.

Experimental setting and software

We employed 5-fold cross-validation to evaluate the robustness and generalizability of the PVDNet model. The dataset was randomly partitioned into 5 folds of equal size. For each fold, the model was trained on 4 folds and validated on the remaining fold. This process was repeated 5 times, ensuring that each fold was used exactly once as the validation set. After completing the 5-fold cross-validation, each of the 5 trained models was independently evaluated on the internal test set. Importantly, these 5 models were not ensembled; instead, their performance metrics were averaged to provide a comprehensive evaluation of the model's performance.

The whole process was performed using Intel® Core™ i7-5930K CPU 3.50 GHz with NVIDIA RTX A4000. The model construction and validation were performed using the Ubuntu 18.04 operating system in the Python 3.7 environment with the open-source library for DL (PyTorch, version 1.10.0; https://pytorch.org/).

The diagnosis performance of readers

The CTPA images in the external validation set were independently evaluated by four radiologists with different levels of expertise from two imaging centers. Four radiologists included a senior radiologist with 20 years of experience in pulmonary vascular diseases in Center 1 (SRPV), a mid-career radiologist with 13 years of experience in pulmonary vascular diseases in Center 2 (MRPV), a junior radiologist with 6 years of experience in pulmonary vascular diseases in Center 1 (JRPV), and a junior resident with 3 years of experience in Center 2 (JRDS).

CTPA evaluations were conducted under a rigorously controlled protocol to ensure methodological robustness. All four radiologists performed blinded evaluations independently, with temporal and spatial separation of reading sessions to eliminate inter-reader communication or bias. A strict blinding protocol was enforced: readers were denied access to clinical metadata (including patient history, laboratory findings, prior imaging reports, and final diagnoses) and were provided exclusively with anonymized full CTPA images devoid of patient identifiers and examination dates. To mitigate sequence-related bias, image datasets were randomized prior to distribution. Evaluations were standardized using predefined visualization parameters, while permitting window width/level adjustments consistent with routine clinical workflows to enhance detection of filling defects. Diagnostic results were independently recorded by each reader using a structured reporting template.

Statistical analysis

All statistical analyses were performed using the Python 3.7 software. The classification performance was determined based on the area under the curve (AUC), sensitivity, specificity, positive predictive value (PPV), and negative predictive value (NPV). Bootstrap (1000 times) was used to estimate 95% confidence intervals (CIs) of each metric. Furthermore, the AUCs of the model and radiologists were compared using DeLong's test. The number of true-positive, false-positive, true-negative, and false-negative findings of classification performance on validation sets was described in a 3×3 contingency table representing the confusion matrix. To further validate the performance of the three-category model, we also evaluated the diagnostic performance of PVDNet in the binary classification setting (PAS vs. PTE). The agreement between model predictions and true labels was examined using the Cohen's kappa coefficient. Consistency was classified as follows[32]: kappa $\geq$ 0.75 indicates good consistency, 0.75 $\geq$ kappa > 0.4 for moderate consistency, and kappa < 0.4 for poor consistency. The details of sample size calculation is shown in the Appendix Material 3.

Ethics approval

This study followed the Declaration of Helsinki and was approved by the Institutional Ethics Committee of China–Japan Friendship Hospital (2022-KY-085). Exemption was granted for obtaining written informed consent from patients.

Role of the funding source

The funder of the study had no role in study design, data collection, data analysis, data interpretation, or writing of the report.

Results

Demographic characteristics

A total of 470 APE patients (male 249, mean age = 65.5 ± 15.2 years), 363 CPE patients (male 235, mean age = 58.4 ± 14.0 years), and 119 PAS patients (male 58, mean age = 51.5 ± 14.6 years) were included in this study. Among 119 PAS patients, 56 cases were confirmed via endovascular biopsy, while 63 cases (52.9%) were diagnosed through surgical pathology. Notably, PAS patients were younger than APE and CPE patients ($F = 52.109$, $p < 0.001$). The characteristics of patients included in the model training, internal test, and external validation are shown in Table 1 and Appendix Table S2. The number of male patients was slightly higher than that of female patients among three groups ($\chi^2 = 7.916$, $p = 0.019$). Besides, there were no statistical differences in cardiopulmonary comorbidities among three groups ($p = 0.668$).

Model performance in the internal test set

The evaluation results for three-category model in the internal test set are shown in Table 2. The PVDNet model predictions and true labels were strongly

	Training set	Internal test	External validation	χ^2/F	p
Number of cases	590	186	176		
Number of centers	3	3	12		
Sex, n (%)					
Male	356 (60.3)	92 (49.5)	94 (53.4)	χ^2 = 7.916	0.019
Female	234 (39.7)	94 (50.5)	82 (46.6)		
Age, years	61.2 ± 14.9	59.4 ± 16.5	62.0 ± 16.0	F = 1.509	0.222
Diagnosis, n (%)					
APE	280 (47.5)	87 (46.8)	103 (58.5)	χ^2 = 16.476	0.002
CPE	246 (41.7)	72 (38.7)	45 (25.6)		
PAS	64 (10.8)	27 (14.5)	28 (15.9)		
Cardiopulmonary co-morbidity, n (%)	306 (51.9)	99 (53.2)	98 (55.7)	χ^2 = 0.810	0.668

PAS = pulmonary artery sarcoma; APE = acute pulmonary thromboembolism; CPE = chronic pulmonary thromboembolism.

Table 1: **Baseline characteristics of patients.**

Category	AUC	Sensitivity	Specificity	PPV	NPV
PAS	0.972 [0.945, 0.994]	0.852 [0.704, 0.971]	0.943 [0.907, 0.975]	0.719 [0.548, 0.875]	0.974 [0.947, 0.994]
APE	0.902 [0.855, 0.944]	0.793 [0.706, 0.873]	0.848 [0.779, 0.917]	0.821 [0.740, 0.901]	0.824 [0.747, 0.894]
CPE	0.900 [0.852, 0.946]	0.806 [0.718, 0.895]	0.895 [0.832, 0.948]	0.829 [0.735, 0.910]	0.879 [0.822, 0.938]

PAS = pulmonary artery sarcoma; APE = acute pulmonary thromboembolism; CPE = chronic pulmonary thromboembolism; AUC = area under curve; PPV = positive predictive value; NPV = negative predictive value.

Table 2: **Model performance in the internal test set.**

correlated, with AUC values of 0.902 (95% CI: [0.855, 0.944]), 0.900 (95% CI: [0.852, 0.946]), and 0.972 (95% CI: [0.945, 0.994]) for APE, CPE, and PAS, respectively. The receiver operating characteristic (ROC) curves are presented in Fig. 3A. Moreover, the model predictions and ground truths in the internal test set were moderately consistent (kappa = 0.687, p < 0.001). The confusion matrix visualizing the number of true-positive, false-positive, true-negative, and false-negative results for the model predictions is shown in Fig. 3B. The binary classification model achieved an AUC of 0.97 for diagnosing PAS (Appendix Fig. S1).

The Gradient-weighted Class Activation Mapping (Grad-CAM)[33] method was used to display the model.

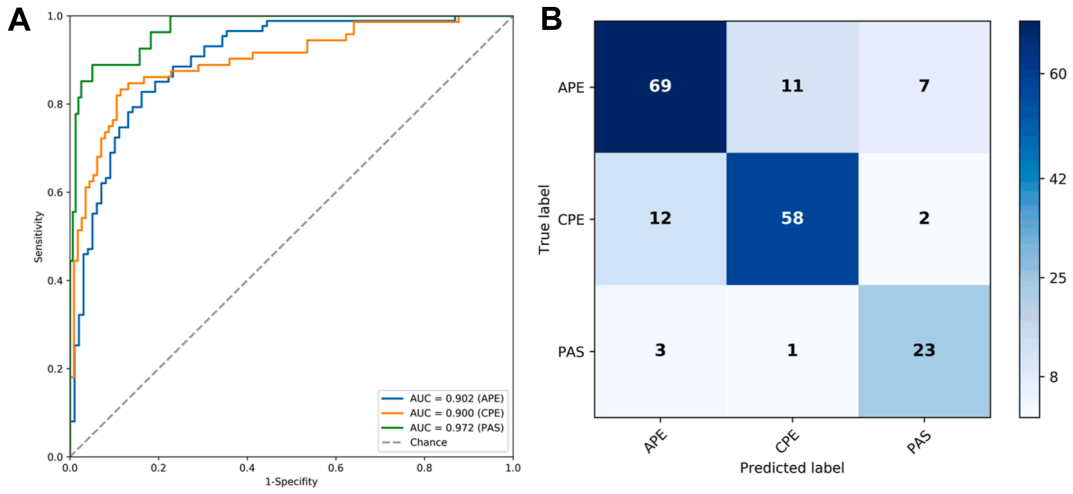

Fig. 3: Model performance of the internal validation set. (A) Receiver operating characteristic curves, (B) confusion matrix (Cohen's kappa, 0.687). PAS = pulmonary artery sarcoma; APE = acute pulmonary thromboembolism; CPE = chronic pulmonary thromboembolism; AUC = area under curve.

The representative Grad-CAM of the model for APE, CPE, and PAS is shown in Fig. 4. Heatmaps illustrated that the method focused on the abnormality in the image when making decisions. The performance metrics for each fold in the internal test set are shown in Appendix Table S3.

Model performance in the external validation set

The evaluation results for three-category model was further evaluated in the external validation set and compared to four radiologists. The results are summarized in Table 3. The model exhibited a good recognition ability for PAS classification, achieving an AUC of 0.973 (95% CI: [0.951, 0.992]), equivalent to the SRPV with an AUC of 0.943 (95% CI: [0.873, 0.997], p = 0.308). Notably, the model's AUC was significantly better than those of the other three readers (JRDS: 0.741, 95% CI: [0.644, 0.833], p < 0.001; JRPV: 0.793, 95% CI: [0.696, 0.884], p < 0.001; MRPV: 0.872, 95% CI: [0.790, 0.951], p < 0.050). Furthermore, the model (AUC: 0.835, 95% CI: [0.775, 0.893]) outperformed the JRDS (AUC: 0.686, 95% CI: [0.613, 0.754]) for APE classification (p < 0.010). In addition, the model had an AUC of 0.809 (95% CI: [0.731, 0.884]) for CPE classification, which was comparable to the JRDS with an AUC of 0.735 (95% CI: [0.657, 0.808], p = 0.230). The ROC curves of the model and four human readers are shown in Fig. 5. For PAS diagnosis, the binary model yielded an AUC of 0.97 (Appendix Fig. S2).

Moreover, the model and the SRPV (kappa = 0.651, p < 0.001) had a moderate agreement, which was the highest among four readers (JRDS kappa = 0.282, JRPV kappa = 0.475, MRPV kappa = 0.554, all p < 0.001). The confusion matrix between the model and each

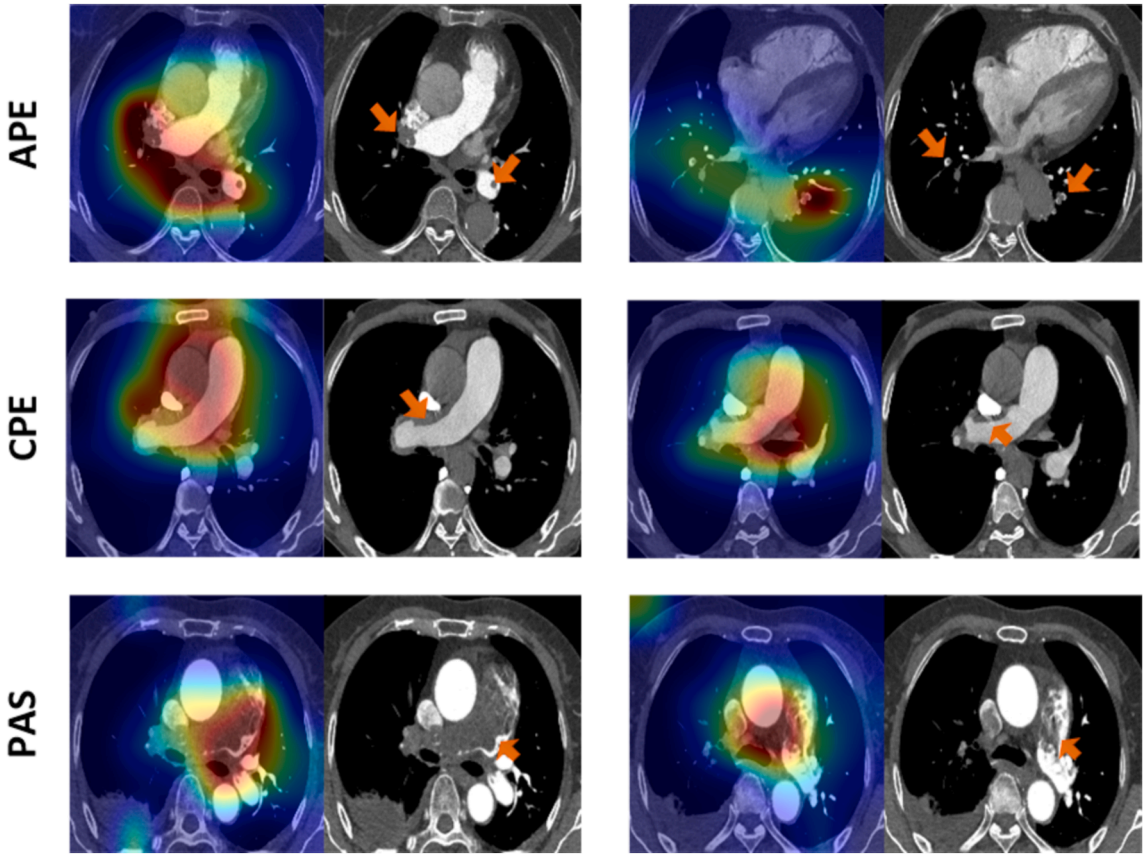

Fig. 4: Heatmaps generated by the Grad-CAM method for APE, CPE, and PAS. The Grad-CAM technique was implemented to generate heatmaps that highlight the specific anatomical regions contributing most significantly to the model's classification decisions. The original CT image (right) of each sample and the corresponding attention heatmap (left) were paired. The red color in the heatmap highlights the activation region associated with the predicted class (the darker the color, the stronger the association). The orange arrows indicate the actual location of the lesion in the original image. For APE, the model emphasized the sharp interface between contrast and non-contrast enhanced regions, while for CPE, it focused on the chronic remodeling features and eccentric narrowing. For PAS, the activation maps highlighted both the central location of the lesion and its unique tissue characteristics, focusing on areas with heterogeneous attenuation. APE = acute pulmonary thromboembolism; CPE = chronic pulmonary thromboembolism; PAS = pulmonary artery sarcoma.

Category	Reader	AUC	Sensitivity	Specificity	PPV	NPV
PAS	PVDNet	0.973 [0.951, 0.992]	0.857 [0.714, 0.971]	0.966 [0.938, 0.993]	0.828 [0.667, 0.962]	0.973 [0.944, 0.994]
	JRDS	0.741 [0.644, 0.833]	0.536 [0.345, 0.714]	0.946 [0.905, 0.980]	0.652 [0.444, 0.850]	0.915 [0.867, 0.956]
	JRPV	0.793 [0.696, 0.884]	0.607 [0.417, 0.792]	0.980 [0.955, 1.000]	0.850 [0.688, 1.000]	0.929 [0.885, 0.967]
	MRPV	0.872 [0.790, 0.951]	0.750 [0.586, 0.909]	0.993 [0.979, 1.000]	0.955 [0.842, 1.000]	0.955 [0.921, 0.987]
	SRPV	0.943 [0.873, 0.997]	0.893 [0.750, 1.000]	0.993 [0.979, 1.000]	0.962 [0.870, 1.000]	0.980 [0.954, 1.000]
APE	PVDNet	0.835 [0.775, 0.893]	0.835 [0.760, 0.903]	0.767 [0.667, 0.857]	0.835 [0.762, 0.900]	0.767 [0.667, 0.866]
	JRDS	0.686 [0.613, 0.754]	0.796 [0.720, 0.871]	0.575 [0.468, 0.685]	0.726 [0.647, 0.800]	0.667 [0.541, 0.783]
	JRPV	0.854 [0.797, 0.903]	0.913 [0.857, 0.963]	0.795 [0.693, 0.889]	0.862 [0.795, 0.925]	0.866 [0.784, 0.941]
	MRPV	0.881 [0.829, 0.929]	0.913 [0.854, 0.961]	0.849 [0.763, 0.924]	0.895 [0.833, 0.949]	0.873 [0.794, 0.942]
	SRPV	0.967 [0.938, 0.991]	0.961 [0.918, 0.991]	0.973 [0.929, 1.000]	0.980 [0.948, 1.000]	0.947 [0.889, 0.988]
CPE	PVDNet	0.809 [0.731, 0.884]	0.644 [0.512, 0.773]	0.885 [0.830, 0.938]	0.659 [0.512, 0.795]	0.879 [0.819, 0.930]
	JRDS	0.735 [0.657, 0.808]	0.578 [0.435, 0.719]	0.893 [0.837, 0.944]	0.650 [0.488, 0.800]	0.860 [0.806, 0.915]
	JRPV	0.873 [0.810, 0.929]	0.822 [0.707, 0.927]	0.924 [0.878, 0.964]	0.787 [0.667, 0.898]	0.938 [0.901, 0.977]
	MRPV	0.910 [0.855, 0.957]	0.889 [0.792, 0.977]	0.931 [0.885, 0.969]	0.816 [0.706, 0.914]	0.961 [0.922, 0.992]
	SRPV	0.955 [0.916, 0.986]	0.956 [0.889, 1.000]	0.954 [0.915, 0.985]	0.878 [0.778, 0.960]	0.984 [0.959, 1.000]

PAS = pulmonary artery sarcoma; APE = acute pulmonary thromboembolism; CPE = chronic pulmonary thromboembolism; JRDS = a junior resident with 3 years of experience; JRPV = a junior radiologist with 6 years of experience in pulmonary vascular diseases; MRPV = a mid-career radiologist with 13 years of experience in pulmonary vascular diseases; SRPV = a senior radiologist with 20 years of experience in pulmonary vascular diseases; AUC = area under curve; PPV = positive predictive value; NPV = negative predictive value.

Table 3: **The diagnosis performance of PVDNet and four radiologists in the external validation set.**

radiologist is shown in Fig. 6. In addition, we compared the consistency of the 4 radiologists in the external validation sets (Appendix Table S4).

Discussion

In this study, a DL model, named as PVDNet, was developed for differentiating PAS and PTE based on CTPA images. There are several important findings: (I) PVDNet achieved the best performance for PAS diagnosis in the internal test set and external validation set. (II) PVDNet demonstrated robust diagnostic performance for PAS comparable to that of a senior radiologist with 20 years of experience in pulmonary vascular diseases. Notably, the model outperformed the other three radiologists in PAS diagnosis. (III) While PVDNet model demonstrates promising overall diagnostic capabilities, its performance in distinguishing APE from CPE requires further optimization (Graphical Abstract).

APE, CPE, and PAS demand radically divergent therapeutic strategies, yet they exhibit overlapping imaging features on CTPA, posing significant diagnostic challenges for clinicians. Although several studies have reported CT characteristics of PAS, including wall eclipsing signs, lesions occupying nearly the entire

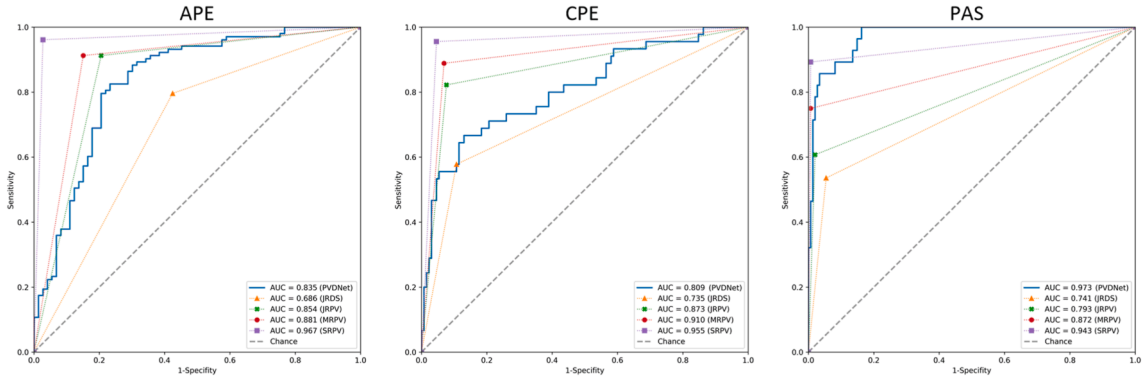

Fig. 5: Receiver operating characteristic curves for APE, CPE, and PAS in external validation set. JRDS = a junior resident with 3 years of experience; JRPV = a junior radiologist with 6 years of experience in pulmonary vascular diseases; MRPV = a mid-career radiologist with 13 years of experience in pulmonary vascular diseases; SRPV = a senior radiologist with 20 years of experience in pulmonary vascular diseases; PAS = pulmonary artery sarcoma; APE = acute pulmonary thromboembolism; CPE = chronic pulmonary thromboembolism; AUC = area under curve.

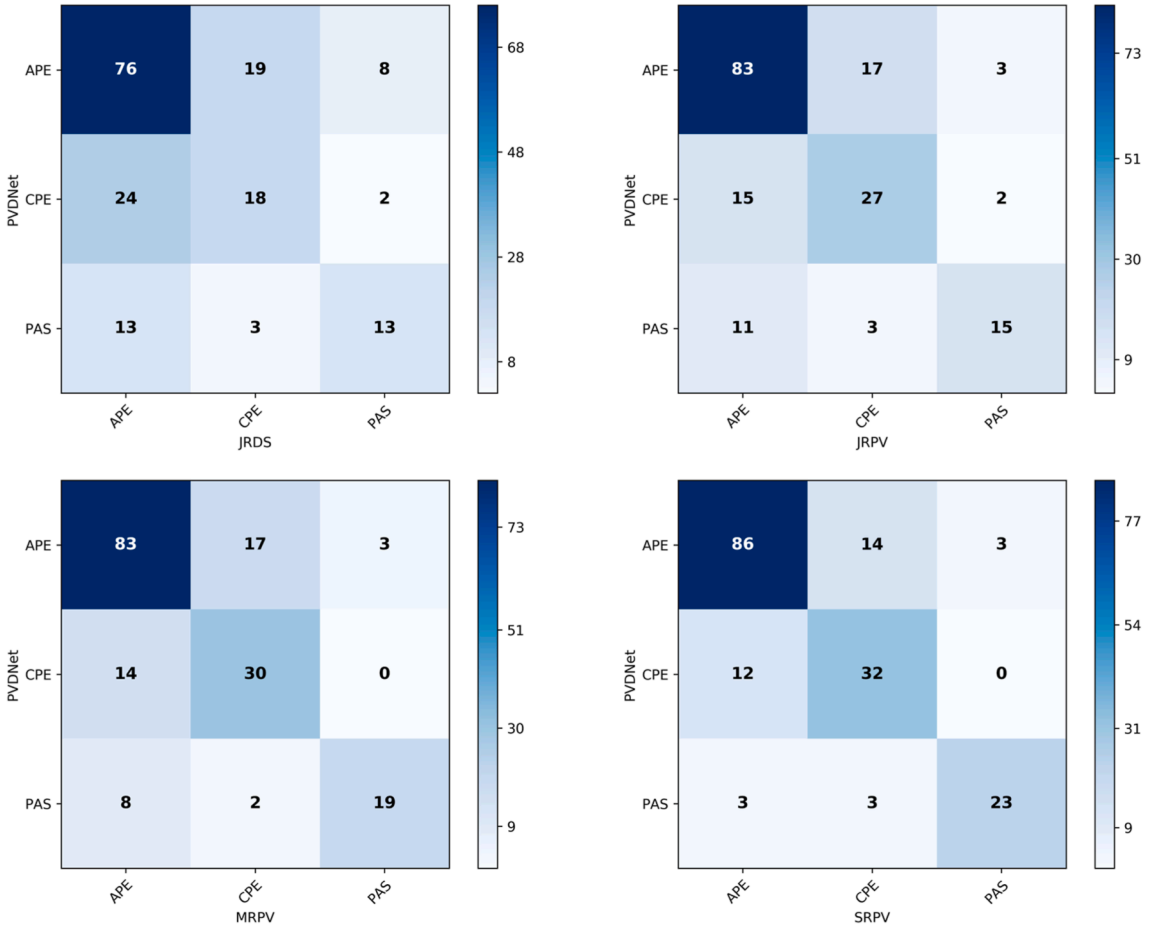

Fig. 6: Confusion matrices between the PDVNet and four human readers in the external validation set. The kappa values for JRDS JRPV, MRPV, and SRPV, were 0.282, 0.475, 0.554, and 0.651, respectively. JRDS = a junior resident with 3 years of experience; JRPV = a junior radiologist with 6 years of experience in pulmonary vascular diseases; MRPV = a mid-career radiologist with 13 years of experience in pulmonary vascular diseases; SRPV = a senior radiologist with 20 years of experience in pulmonary vascular diseases; PAS = pulmonary artery sarcoma; APE = acute pulmonary thromboembolism; CPE = chronic pulmonary thromboembolism.

lumen at the proximal pulmonary arteries level, expansion of pulmonary arteries, and extraluminal extensions,[16,34,35] these findings were derived from small sample sizes. Furthermore, previous studies revealed that most PAS cases exhibited central-type involvement (main, left or right, or lobar pulmonary arteries).[12,13,16] Currently, no imaging-based models exist to differentiate APE, CPE, and PAS. To address this gap, we developed the PVDNet, a novel diagnostic framework to classify these three entities. To the best of our knowledge, our study includes the largest cohort of PAS patients to date. The PVDNet framework employs a pre-trained ResNet-50 backbone enhanced with domain-specific adaptations for pulmonary vascular disease differentiation on CTPA imaging. ResNet-50 can handle very deep network structures, effectively mitigating the issue of gradient vanishing. Based on ResNet-50, we introduced three modifications: (1) max-pooling-based feature aggregation to prioritize discriminative spatial patterns and suppress noise, particularly vital for rare PAS detection; (2) a fine-grained classification head (fully connected layer + softmax) optimized for APE, CPE, and PAS stratification; and (3) integrated Grad-CAM modules enabling interpretable saliency mapping aligned with radiologists' diagnostic focus areas. This feature enables radiologists to comprehend the basis of the model's predictions, thereby enhancing confidence in its clinical applicability. Additionally, hyperparameters such as learning rate, batch size, and loss function weighting were carefully tuned using cross-validation to optimize performance. These adaptations enhanced PVDNet's generalization and clinical utility. To address severe class imbalance (PTE: PAS = 7:1), we implemented two-fold oversampling of the PAS dataset in the training process. We also replaced the standard random sampling with class-weighted random sampling, where weights

were inversely proportional to class frequencies and integrated class-balanced loss to prioritize learning from underrepresented classes. Moreover, we used a five-fold cross-validation method for model development, which not only increased the effective utilization of training samples but also mitigated the impact of data imbalance on model performance.

Our study leveraged CTPA datasets from 15 centers, utilizing diverse CT scanners with varying technical parameters. While this heterogeneity enhances the generalizability of PVDNet, it also introduces potential variability in image quality and resolution. To mitigate these effects, we implemented rigorous preprocessing steps, including standardized window settings, lung region segmentation via a validated DL-based tool, and min-max normalization to harmonize grayscale distributions. These measures aimed to reduce inter-scanner biases and ensure consistent input for the model. However, residual variability may persist due to differences in contrast injection protocols, reconstruction algorithms, or motion artifacts across centers. For instance, subtle differences in vascular enhancement or noise levels could theoretically influence feature extraction, particularly for discriminating APE and CPE, where imaging findings are more nuanced. Notably, PVDNet's performance in PAS classification remained robust across both internal and external validation sets, suggesting that the model's reliance on salient morphological features may be less susceptible to technical variations. In contrast, the slightly lower performance for APE/CPE differentiation in the external validation set may reflect the compounded effects of inter-center heterogeneity and class imbalance. Future studies can utilize tools such as ComBat or other imaging harmonization methods to address this issue.

The PVDNet model demonstrated superior diagnostic performance for PAS across both internal and external validation cohorts. In the internal test set, PVDNet achieved AUC of 0.972, 0.902, and 0.900 for PAS, APE, and CPE respectively, highlighting its robust recognition capability across three types of pulmonary vascular diseases. Notably, the model demonstrated exceptional accuracy in PAS detection, suggesting potential clinical value in reducing PAS diagnostic delays. External validation results confirmed the model's generalizability, with PVDNet achieving an AUC of 0.973 for PAS classification. We also found that the diagnostic performance of PAS in the two-class scenario did not differ significantly from that in the three-category classification across both internal and external test sets. Nevertheless, distinguishing between APE and CPE is clinically important due to differences in their diagnostic and treatment strategies. However, binary classification models are unable to differentiate between APE and CPE. Comparative analysis revealed comparable performance between PVDNet and a senior radiologist with 20 years of experience in pulmonary vascular diseases. Moreover, PVDNet model demonstrated significantly higher sensitivity than those of three less experienced radiologists, indicating its potential to enhance diagnostic capability in clinical settings lacking specialized expertise. The strong agreement between model predictions and final clinical diagnoses demonstrates the model's reliability and clinical utility.

Notably, PVDNet performs differently in different diagnostic tasks. PVDNet performed best in the diagnosis of PAS, whereas it did not perform as well as experienced radiologists in the differentiation of APE and CPE. This performance discrepancy indicates that the imaging features of APE and CPE may be more complex and subtle than those of PAS, requiring radiologists to integrate clinical experience and anatomical knowledge for comprehensive judgment. In distinguishing between APE and CPE, radiologists not only focus on the morphological characteristics of filling defects but also consider changes in vascular wall structure, bronchovascular relationships, and secondary alterations in lung parenchyma, among other factors. The integration of these complex features may pose a challenge for current PVDNet model. Furthermore, single time-point CTPA analysis fails to capture dynamic transitions from acute to chronic phases, and future longitudinal cohort based on CHOICE cohort should construct a multitemporal trajectory model of PTE for predicting disease progression.

Morever, The PVDNet model exhibited diminished diagnostic performance for APE and CPE in external validation set compared with internal test set, primarily attributable to imbalance in disease distribution between cohorts. The proportion of APE patients in the external validation set is higher, while the proportion of CPE patients is lower. In addition, the external validation set is characterized by higher heterogeneity than the internal test set (12 centers vs. 3 centers). This difference highlights the importance of external validation and provides a more realistic assessment of the model's performance in different contexts. While our current study demonstrated robust performance of PVDNet in differentiating PAS from PTE across diverse patient populations, we acknowledge the need for future investigations to specifically evaluate the potential impact of patient sex on model performance. We did not perform subgroup analyses by sex due to sample size limitations in certain subgroups. Given known sex differences in pulmonary vascular physiology and disease presentation, future studies with larger sample sizes should systematically assess whether sex-specific variations in imaging features or disease manifestations influence the model's diagnostic accuracy. This could include developing sex-stratified models or incorporating sex as an additional input feature to optimize performance across all populations.

This study has some limitations that should be acknowledged. First, although PVDNet model demonstrates promising discriminative performance in differentiating PAS from PTE, its development relied on retrospective analysis of a subset from the CHOICE study. Prospective validation can offer more robust evidence to underpin the clinical utility of the PVDNet model and further facilitate model optimization. Second, our study's PAS proportion (12.5%) reflects intentional case collection at referral centers and should not be interpreted as population incidence. The elevated PAS proportion enables robust model development for this rare but critical diagnosis. While the pretest probability differs in general practice, PVDNet's high specificity (external validation) ensures it will not substantially increase false positives in low-prevalence settings. Future studies should validate the diagnostic efficacy of PVDNet in real clinical settings. Third, the current model processes only CTPA imaging data without other clinical data such as symptoms and biomarkers (including D-dimer or brain natriuretic peptide). Integration of these multimodal data could improve diagnostic capabilities. Fourth, although endovascular pulmonary artery tumors, often consisting of tumor thrombi, are more common in patients with cancer,[36] the model's performance in distinguishing tumor thrombi from PTE remains unevaluated due to insufficient pathologically confirmed cases. As more pathologically confirmed tumor thrombi cases accumulate, expanding the model to identify this entity will be a crucial research direction. Fifth, while advanced modalities like MRI and PET/CT provide complementary diagnostic value,[12,17] their limited clinical adoption constrained integration in this study. Future iterations of PVDNet could integrate multimodal imaging inputs to improve diagnostic accuracy. Sixth, the capacity of the model to enhance radiologists' diagnostic performance through human-AI collaboration remains unstudied. Future studies should compare diagnostic accuracy across three paradigms: radiologist-only, AI-only, and AI-assisted interpretation. This will determine whether AI can effectively reduce the diagnostic gap between radiologists of different specialization levels. In conclusion, the PVDNet model based on CTPA shows encouraging results in differentiating between PAS and PTE, and achieves a discriminatory ability comparable to that of senior radiologists specializing in pulmonary vascular diseases in the external validation set, providing a potential auxiliary tool for the diagnosis of pulmonary vascular diseases.

Contributors

Linfeng Xi, Anqi Liu, and Han Kang has full access to all the data in the study and takes responsibility for the integrity of the data and accuracy of the data analysis. Dr. Min Liu and Dr. Zhenguo Zhai had final responsibility for the decision to submit for publication. **Concept and design:** Min Liu and Zhenguo Zhai. **Acquisition data:** Linfeng Xi, Anqi Liu, Xiaoyan Li, Xiaojuan Guo, Minjie Lu, Hui Liu, Yinzhu Chen, Heng Ma, Yinsu Zhu, Yu Deng, Liqing Peng, Fajiu Li, Ziyang Zhu, Lihua Wang, Xin Chen, Hong Yu, Hongjie Hu, Cong Shen, Xiaoyan Lei, Zixian Chen, Xincao Tao, Xiaopeng Liu, and Zhenguo Zhai. **Analysis and interpretation of data:** Linfeng Xi, Anqi Liu, Han Kang, Yifei Ni, Jianping Wang, and Hongyi Wang. **Drafting of the manuscript:** Linfeng Xi, Anqi Liu, and Han Kang. **Statistical analysis:** Linfeng Xi, Han Kang, and Hongyi Wang. **Administrative, technical or material support:** Min Liu, Qiang Huang, Yanan Zhen, Rongguo Zhang, and Wanmu Xie. **Supervision:** Zhenguo Zhai.

Data sharing statement

Data generated or analyzed during the study are available from the corresponding author upon request.

Declaration of interests

All authors report no conflict of interest.

Acknowledgements

We would like to thank all the participants, investigators, and healthcare professionals for making the study possible.

Appendix A. Supplementary data

Supplementary data related to this article can be found at https://doi.org/10.1016/j.lanwpc.2025.101625.

References

1 Konstantinides SV, Meyer G, Becattini C, et al. 2019 ESC Guidelines for the diagnosis and management of acute pulmonary embolism developed in collaboration with the European Respiratory Society (ERS). *Eur Heart J*. 2020;41(4):543–603.
2 Ho ATN, Bellamy N, Naydenov SK. Trends in mortality of acute pulmonary embolism. *Semin Respir Crit Care Med*. 2021;42(2):171–175.
3 Zhai Z, Wang D, Lei J, et al. Trends in risk stratification, in-hospital management and mortality of patients with acute pulmonary embolism: an analysis from the China pUlmonary thromboembolism REgistry Study (CURES). *Eur Respir J*. 2021;58(4):2002963.
4 Klok FA, Mos IC, van Kralingen KW, Vahl JE, Huisman MV. Chronic pulmonary embolism and pulmonary hypertension. *Semin Respir Crit Care Med*. 2012;33(2):199–204.
5 Winter MP, Schernthaner GH, Lang IM. Chronic complications of venous thromboembolism. *J Thromb Haemost*. 2017;15(8):1531–1540.
6 Hirakawa K, Yamamoto E, Takashio S, et al. Balloon pulmonary angioplasty in chronic thromboembolic pulmonary hypertension. *Cardiovasc Interv Ther*. 2022;37(1):60–65.
7 Michaud E, Pan M, Aggarwal V. Catheter-based therapies in acute and chronic pulmonary embolism. *Curr Opin Cardiol*. 2021;36(6):704–710.
8 Wyler von Ballmoos MC, Chan EY, Reardon MJ. Imaging and surgical treatment of primary pulmonary artery sarcoma. *Int J Cardiovasc Imaging*. 2019;35(8):1429–1433.
9 Li J, Liu L, Song LX, et al. Clinical features and outcomes of pulmonary artery sarcoma. *Heart Lung Circ*. 2022;31(2):230–238.
10 Kronzer E, Robinson SI, Collins DA, McBane RD 2nd. Primary pulmonary artery sarcoma versus pulmonary thromboembolism: a multimodal imaging comparison. *J Thromb Thrombolysis*. 2021;52(4):1129–1132.
11 Chang S, Hur J, Im DJ, et al. Dual-energy CT-based iodine quantification for differentiating pulmonary artery sarcoma from pulmonary thromboembolism: a pilot study. *Eur Radiol*. 2016;26(9):3162–3170.
12 Liu M, Luo C, Wang Y, et al. Multiparametric MRI in differentiating pulmonary artery sarcoma and pulmonary thromboembolism: a preliminary experience. *Diagn Interv Radiol*. 2017;23(1):15–21.
13 Kim C, Kim MY, Kang JW, Song JS, Lee KY, Kim SS. Pulmonary artery intimal sarcoma versus pulmonary artery thromboembolism: CT and clinical findings. *Korean J Radiol*. 2018;19(4):792–802.
14 Xi XY, Gao W, Gong JN, et al. Value of (18)F-FDG PET/CT in differentiating malignancy of pulmonary artery from pulmonary thromboembolism: a cohort study and literature review. *Int J Cardiovasc Imaging*. 2019;35(7):1395–1403.

15 Liu MX, Ma ZH, Jiang T, et al. Differential diagnosis of pulmonary artery sarcoma and central chronic pulmonary thromboembolism using CT and MR images. *Heart Lung Circ*. 2018;27(7):819–827.
16 Guo R, Yang H, Xi L, et al. Comparison of pulmonary artery sarcoma and pulmonary thromboembolism according to clinical and computed tomography pulmonary angiography and magnetic resonance imaging characteristics: a single-center retrospective study. *Quant Imaging Med Surg*. 2024;14(2):1686–1698.
17 Ren J, Li H, Zhang Q, et al. Clinical utility of (18)F-FDG PET/CT imaging in patients with pulmonary artery sarcoma. *EJNMMI Res*. 2022;12(1):18.
18 Liu W, Liu M, Guo X, et al. Evaluation of acute pulmonary embolism and clot burden on CTPA with deep learning. *Eur Radiol*. 2020;30(6):3567–3575.
19 Zhang H, Cheng Y, Chen Z, et al. Clot burden of acute pulmonary thromboembolism: comparison of two deep learning algorithms, Qanadli score, and Mastora score. *Quant Imaging Med Surg*. 2022;12(1):66–79.
20 Wang ZC, Fan ZZ, Liu XY, et al. Deep learning for discrimination of hypertrophic cardiomyopathy and hypertensive heart disease on MRI native T1 maps. *J Magn Reson Imaging*. 2024;59(3):837–848.
21 Chen L, Fu G, Jiang C. Deep learning-derived 12-lead electrocardiogram-based genotype prediction for hypertrophic cardiomyopathy: a pilot study. *Ann Med*. 2023;55(1):2235564.
22 Chao CJ, Jeong J, Arsanjani R, et al. Echocardiography-based deep learning model to differentiate constrictive pericarditis and restrictive cardiomyopathy. *JACC Cardiovasc Imaging*. 2024;17(4):349–360.
23 Li M, Ling R, Yu L, et al. Deep learning segmentation and reconstruction for CT of chronic total coronary occlusion. *Radiology*. 2023;306(3):e221393.
24 Zhou Z, Gao Y, Zhang W, et al. Deep learning-based prediction of percutaneous recanalization in chronic total occlusion using coronary CT angiography. *Radiology*. 2023;309(2):e231149.
25 Collins GS, Moons KGM, Dhiman P, et al. TRIPOD+AI statement: updated guidance for reporting clinical prediction models that use regression or machine learning methods. *BMJ*. 2024;385:e078378.
26 Sun H, Liu M, Liu A, et al. Developing the lung graph-based machine learning model for identification of fibrotic interstitial lung diseases. *J Imaging Inform Med*. 2024;37(1):268–279.
27 Li L, Qin L, Xu Z, et al. Using artificial intelligence to detect COVID-19 and community-acquired pneumonia based on pulmonary CT: evaluation of the diagnostic accuracy. *Radiology*. 2020;296(2):E65–E71.
28 He K, Zhang X, Ren S, Sun J. Deep residual learning for image recognition. In: *2016 IEEE Conference on Computer Vision and Pattern Recognition (CVPR); 2016 27–30 June*. 2016:770–778.
29 Deng J, Dong W, Socher R, Li LJ, Kai L, Li F-F. ImageNet: a large-scale hierarchical image database. In: *2009 IEEE Conference on Computer Vision and Pattern Recognition; 2009 20–25 June*. 2009:248–255.
30 Cui Y, Jia M, Lin TY, Song Y, Belongie S. Class-balanced loss based on effective number of samples. In: *2019 IEEE/CVF Conference on Computer Vision and Pattern Recognition (CVPR); 2019 15–20 June*. 2019:9260–9269.
31 Isensee F, Jäger P, Wasserthal J, et al. *Batchgenerators - A Python Framework for Data Augmentation (0.19.6)*. Zenodo; 2020.
32 Landis JR, Koch GG. The measurement of observer agreement for categorical data. *Biometrics*. 1977;33(1):159–174.
33 Selvaraju RR, Cogswell M, Das A, Vedantam R, Parikh D, Batra D. Grad-CAM: visual explanations from deep networks via gradient-based localization. In: *2017 IEEE International Conference on Computer Vision (ICCV); 2017 22–29 October*. 2017:618–626.
34 Gan HL, Zhang JQ, Huang XY, Yu W. The wall eclipsing sign on pulmonary artery computed tomography angiography is pathognomonic for pulmonary artery sarcoma. *PLoS One*. 2013;8(12):e83200.
35 Cox JE, Chiles C, Aquino SL, Savage P, Oaks T. Pulmonary artery sarcomas: a review of clinical and radiologic features. *J Comput Assist Tomogr*. 1997;21(5):750–755.
36 Gimbel IA, Mulder FI, Bosch FTM, et al. Pulmonary embolism at autopsy in cancer patients. *J Thromb Haemost*. 2021;19(5):1228–1235.